www.czasopisma.pan.pl PAN POLSKA AKADEMIA NAUK www.journals.pan.pl

Arch. Metall. Mater. **65** (2020), 3, 1111-1116

DOI: 10.24425/amm.2020.133226

JEONG HYUN KIM[1], MYEONGJUN JI[1], CHEOL-HUI RYU[1], YOUNG-IN LEE[1,2*]

EFFECT OF PYROLYSIS CONDITIONS ON THE PHYSICOCHEMICAL PROPERTIES OF GRAPHITIC CARBON NITRIDE FOR VISIBLE-LIGHT-DRIVEN PHOTOCATALYTIC DEGRADATION

Graphitic carbon nitride (g-C_3N_4) is an attractive photocatalyst, however, its practical photocatalytic applications are still faced with huge challenges. The aim of this research is to identify the correlation between synthetic conditions and properties of the g-C_3N_4 and derive an optimum synthesis condition for improving photocatalytic activities of the g-C_3N_4. In this study, novel and versatile g-C_3N_4 nanosheets were synthesized by the simple thermal pyrolysis of urea. In the synthesis process, the pyrolysis temperature and the heating rate, which can have the most significant influence on the structures and properties of g-C_3N_4, were set as variables, and the effects were systematically investigated. When synthesized at a relatively high temperature, the amount of material being synthesized is reduced, however it has been found to represent optical properties suitable for highly efficient photocatalyst by the increase in the thickness and defects formed in the g-C_3N_4 nanosheets. The photocatalytic degradation experiment of MB dyes indicated that the highest degradation of 95.2% after the reaction for 120 min was achieved on the g-C_3N_4 nanosheets synthesized at 650°C.

Keywords: g-C_3N_4; Pyrolysis; Polymerization; Synthesis condition; Photocatalysis

1. Introduction

In recent years, there has been increasing interest in the study of heterogeneous photocatalysis which has been utilized to directly harvest, convert and store renewable solar energy to produce sustainable and green solar fuels and water and air purification [1-3]. Titanium dioxide (TiO_2) has been one of the most outstanding photocatalysts during recent decades because of an excellent photocatalytic activity under ultraviolet (UV) irradiation, however, TiO_2 can be activated only under UV irradiation due to its relatively large band gap ($E_g = 3.0 \sim 3.2$ eV). Various researches including cation or anion doping and surface modification for the utilization of visible light have been carried out to overcome the limitation of the TiO_2 [4-6]. From a different point of view, non-TiO_2-based photocatalysts with visible light response including metal oxides and sulfides have been actively studied [7-11].

Graphitic carbon nitride (g-C_3N_4), as one of the most promising visible-light-driven photocatalysts with an appropriate band gap, outstanding layered porous structure, low cost, good chemical stability and non-toxicity has received extensive attention in energy conversion and organic pollutant degradation [12,13]. It is well known that g-C_3N_4 can be easily synthesized by thermal pyrolysis of organic precursors such as melamine, cyanamide and urea, however, its practical photocatalytic applications are still faced with huge challenges, such as insufficient visible light absorption, low electron mobility, high recombination rate of photogenerated charge carriers. Although the limitations can be improved by developing unique nanostructures and by implementing heterojunctions of the g-C_3N_4 with other nanomaterials [12-14], it should fundamentally be preceded by maximizing the true characteristics of the g-C_3N_4 to realize practical photocatalytic applications.

The physicochemical, optical and electrical properties of the g-C_3N_4 depend largely on the structure and composition characteristics including crystal structure, crystallinity and impurity level which are mainly determined by synthetic conditions. Therefore, it is necessary to identify the correlation between the process condition and structure and property of the g-C_3N_4 and derive the optimum synthesis conditions. In this study, our goal is to investigate the effect of the synthesis condition on the properties of the g-C_3N_4 and to determine an optimum synthesis condition for the g-C_3N_4 photocatalyst with the best photocatalytic efficiency. The g-C_3N_4 was synthesized by the

[1] SEOUL NATIONAL UNIVERSITY OF SCIENCE AND TECHNOLOGY, DEPT. OF MATERIALS SCIENCE AND ENGINEERING, SEOUL 01811, REPUBLIC OF KOREA
[2] SEOUL NATIONAL UNIVERSITY OF SCIENCE AND TECHNOLOGY, INSTITUTE OF POWDER TECHNOLOGY, SEOUL 01811, REPUBLIC OF KOREA

* Corresponding author: youngin@seoultech.ac.kr

simple thermal pyrolysis of urea under ambient pressure without additives. In the synthesis process, the pyrolysis temperature and the heating speed, which can have the most significant influence on the structure and properties of g-C_3N_4, were set as variables, and the effects were systematically investigated.

2. Experimental

Typically, 10 g of the urea powder (>99.5%, Sigma-Aldrich) were added into a covered crucible, and then it was dried at 80°C for 24 h under vacuum condition to remove volatile substances. The powder was heated to 550, 600, 650 and 700°C in air at a heating rate of 2, 5 and 10°C/min and maintained at each temperature for 3 h in an alumina crucible with a cover in aluminum or copper foils. Thus yellowish powder was obtained. The crystal structures and crystallite sizes of the samples were characterized by X-ray diffractometer (XRD, X'Pert^3 Powder, PANalytical, Netherlands) with CuKα radiation. XRD patterns were obtained from 10° to 90° of 2θ at a scanning rate of 4° min^{-1}. The morphology of the samples was observed by field emission scanning electron microscopy (FE-SEM, S-4800, Hitachi, Japan) and high-resolution transmission electron microscopy (HR-TEM, JEM-2100F, JEOL, Japan). UV-vis diffuse reflection spectra were obtained by an UV-vis spectrophotometer (SHIMADZU UV-2600, SHIMADZU Japan) in the range of 200-800 nm.

The photocatalytic activities of the samples were investigated by the degradation experiments of methylene blue (MB). The activity was confirmed with the color change of the MB during the photocatalytic degradation based on the Beer-Lambert law which is the linear relationship between absorbance and concentration of an absorbing species [15]. Photocatalytic experiments were carried out by adding 0.05 g of samples to 100 mL of 3 × 10^{-5} M MB aqueous solution and using a solar simulator equipped with a 300 W xenon lamp which a filter with a 420 nm cut-off was employed (Newport FSQ-GG395). Before the irradiation, the mixtures were kept in the dark for 80 min to reach the adsorption-desorption equilibrium among the photocatalyst, MB and water. The prepared solutions were irradiated using the lamp with being magnetically stirred in a water bath at 25°C. A series of certain volume of samples were withdrawn at selected times for analysis and were centrifuged for a measurement. The remaining MB concentration was confirmed by the UV/Vis spectrometer.

3. Results and discussion

Fig. 1 shows the amount of the products synthesized by the thermolysis of the urea at different temperatures and heating rates. As shown in Fig. 1, both the thermal pyrolysis temperature and the heating speed for the synthesis of g-C_3N_4 affected the amount of the synthesized products, however, the effect of the pyrolysis temperature was found to be more pronounced. The largest amount was synthesized at a temperature of 550°C, similar to that of the previously reported study [16,17], but the amount was about one-tenth of the theoretical value, and the synthesized amount was also reduced as the temperature increased because the thermal decomposition of the urea proceeds faster as the temperature increases, and the crystallization of g-C_3N_4 becomes more difficult because the saturated vapor pressure increases at higher temperatures. Crystal structures of the prepared samples are recorded by XRD. As illustrated in Fig. 2, all samples have two diffraction peaks indicating a typical graphic layered structure. The diffraction peaks of all samples can be indexed to crystal plane of pure hexagonal g-C_3N_4 (JCPDS No. 87-1526). The peak located at 2θ of 27° is attributed to (002) plane which is related to stack the conjugated aromatic system up corresponding well to the interlayer d-spacing (0.336 nm) of the g-C_3N_4 [16,17]. The weak peak also appeared at 2θ of 13°,

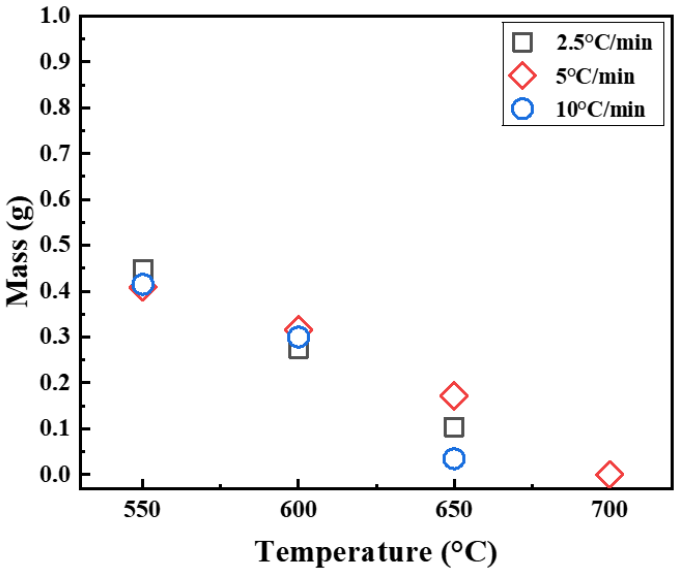

Fig. 1. The amount of the products synthesized by the pyrolysis of the urea as a function of pyrolysis temperature and heating rate

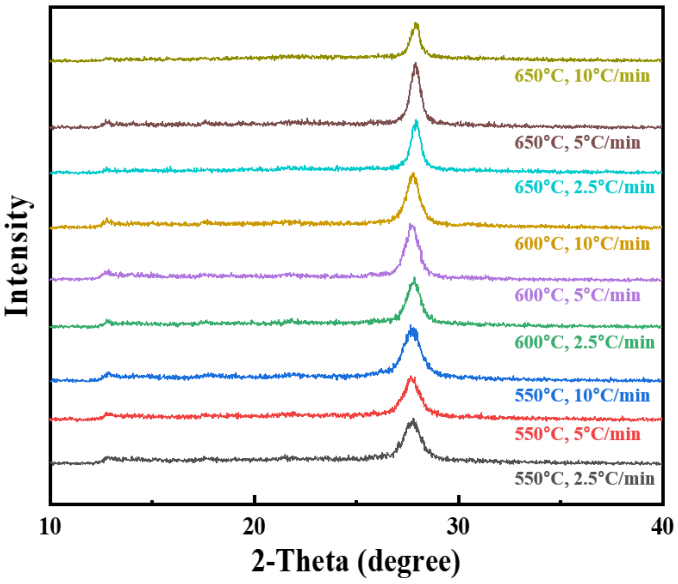

Fig. 2. XRD patterns of the products synthesized by the pyrolysis of urea at various temperatures and heating rates

corresponding to the (100) plane with interplanar distance of 0.672 nm in g-C_3N_4. The peak intensities of the (100) plane showed a tendency to decrease as the synthesis temperature increased, as more defects were formed in interplanar structures at higher synthetic temperatures. The corresponding crystallite size was calculated from the (002) diffraction peak using Scherrer equation [18] to confirm the thickness of the synthesized g-C_3N_4 and the values are arranged in table 1. As shown in table 1, the crystallite size increased as the synthetic temperature increased. This means that the thickness of the synthesized product increases as the pyrolysis temperature increases. These results can be explained by the change in a growth mechanism. If synthesized at a relatively low temperature, the concentration of growth species may be kept low after a nucleation of g-C_3N_4 due to rapid nucleation by low vapor pressure and the slow decomposition of the urea. In this case, the growth process is controlled by the diffusion of growth species which promotes the morphology with lowest surface energy. On the other hand, when synthesized at relatively high temperatures, the growth is dependent on the surface process (adsorption and incorporation of growth species onto the solid surface) due to the relatively slow rate of nucleation and the rapid decomposition of urea and, thus the growth of g-C_3N_4 can occur in all crystal directions.

TABLE 1

The crystallite sizes of the synthesized g-C_3N_4 samples calculated from the (002) diffraction peak using Scherrer equation

Temperature	Ramping rate	Crystallite size
550°C	2.5°C/min	10.5 nm
	5°C/min	11.1 nm
	10°C/min	10.0 nm
600°C	2.5°C/min	12.5 nm
	5°C/min	11.9 nm
	10°C/min	12.3 nm
650°C	2.5°C/min	14.8 nm
	5°C/min	14.6 nm
	10°C/min	15.8 nm

FE-SEM images show the morphology and thickness differences of the g-C_3N_4 synthesized at various conditions. As shown in Fig. 3, platelet-like shapes are found in all samples which can be attributed to the result of anisotropic crystal growth

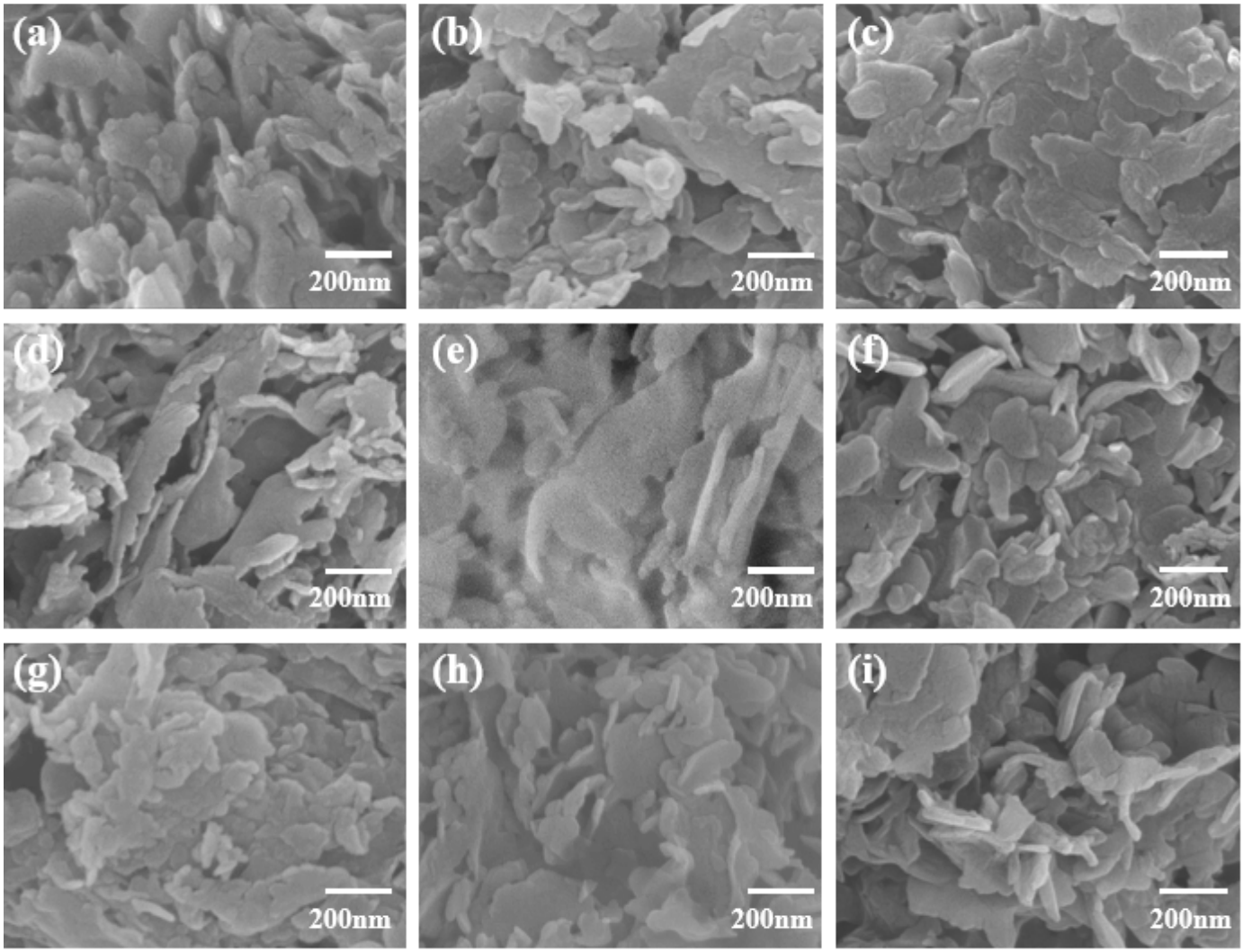

Fig. 3. FE-SEM images of the g-C_3N_4 samples synthesized at various conditions: (a) 550°C, 2.5°C/min, (b) 600°C, 2.5°C/min, (c) 650°C, 2.5°C/min, (d) 550°C, 5°C/min, (e) 600°C, 5°C/min, (f) 650°C, 5°C/min, (g) 550°C, 10°C/min, (h) 600°C, 10°C/min, and (i) 650°C, 10°C/min

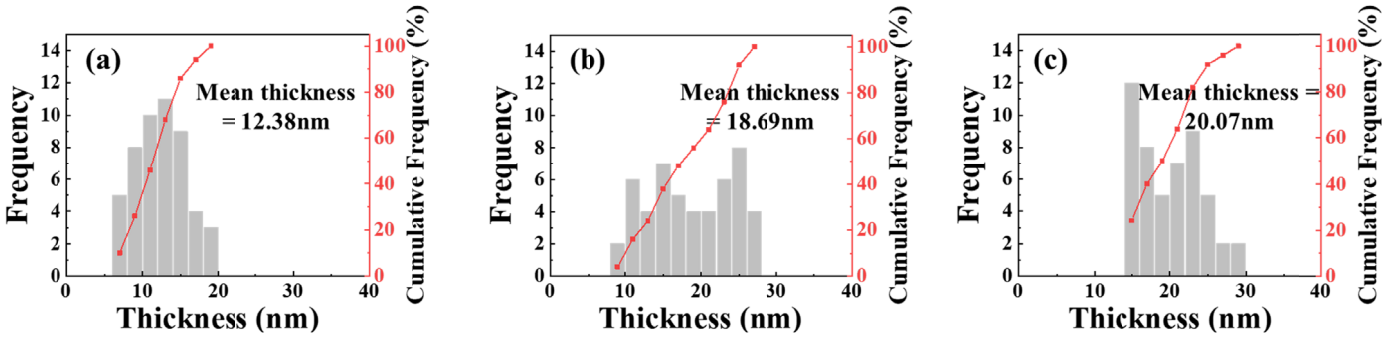

Fig. 4. The graphs showing the thickness distributions and averages of g-C_3N_4 nanosheets synthesized at (a) 550°C, (b) 600°C and (c) 650°C with a heating rate of 5°C/min

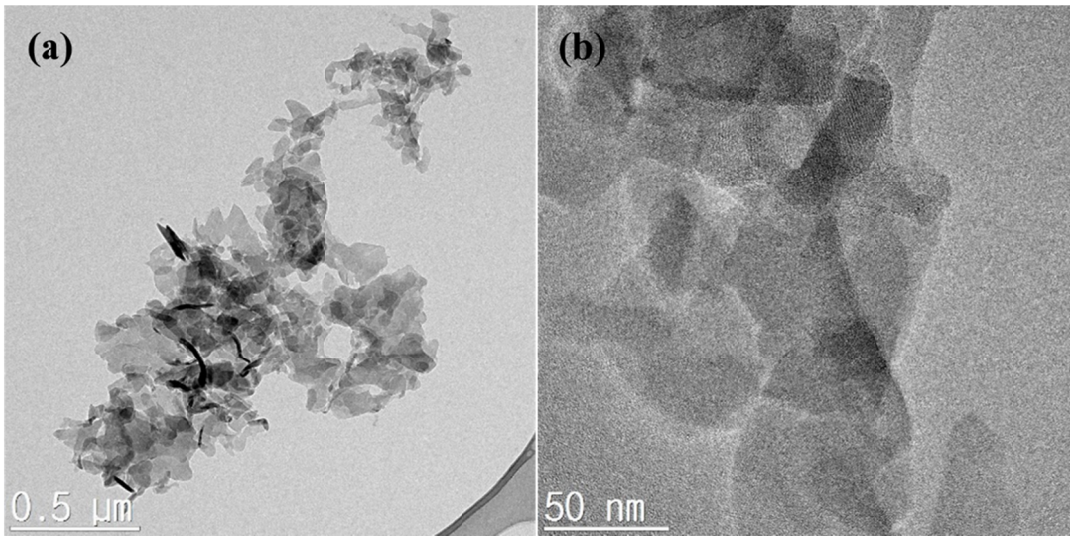

Fig. 5. (a) low and (b) high magnification TEM images of the g-C_3N_4 nanosheets obtained at 650°C with the heating rate of 5°C/min

during the pyrolysis process. All samples had the size dimension in the range of 50-250 nm and thickness of 5-30 nm. For the samples, there isn't obvious difference in the shapes and diameters, however, the g-C_3N_4 nanosheets thickened clearly as the increase in the temperature. The obtained micrographs were processed and analyzed by the software imageJ to determine the average thickness of the nanosheets. The size distribution and average thickness were generated by manually selecting and measuring around 50 nanosheets. As shown in Fig. 4, the average values of the nanosheets synthesized at 550°C, 600°C and 650°C under the heating rate of 5°C were 12.3, 18.7 and 20.1 nm, respectively. This trend on thickness changes is well consistent with the crystallite sizes calculated by Scherrer equation. The morphologies and microstructures of the g-C_3N_4 nanosheets were clearly visualized using TEM. Fig. 5 shows the low and high magnification TEM images of the g-C_3N_4 nanosheet obtained at 650°C with the heating rate of 5°C/min. It was confirmed that the g-C_3N_4 particles were sheet structures with a diameter of 50-200 nm and thickness of below 20 nm.

The optical absorption characteristics of the g-C_3N_4 nanosheets were investigated by an UV-vis spectrometer and presented in Fig. 6. All the samples absorbed the visible light strongly which could be responsible for the visible-light-driven photocatalytic activity. The absorption thresholds clearly shift to longer wavelengths and the visible light absorption intensities are improved with increasing pyrolysis temperatures. This can be attributed to the formation of structural defects in the g-C_3N_4 nanosheets and the reduced band gap energy due to thick thickness of the g-C_3N_4 nanosheets when they were synthesized at high temperatures. The photocatalytic activities of the g-C_3N_4 nanosheets which were synthesized at different temperatures are investigated by the degradation of MB under visible-light irradiation ($\lambda > 420$ nm). Fig. 7(a-c) shows adsorption spectra of MB solutions in the presence of g-C_3N_4 nanosheets under visible light as a function of time. These graphs clearly show that the maximum absorbance of 665 nm decreases greatly after irradiation. The comparison of MB photocatalytic degradation by the g-C_3N_4 against irradiation time is shown in Fig. 7(d). Here, C/C_0 changes over reaction time are used to evaluate the photocatalytic degradation rates, where C_0 is the original concentration of dyes and C is the concentration of filtrates taken during the reactions. A blank test without any photocatalyst was also executed and demonstrated that the photodegradation of RhB was extremely slight, indicating that the photolysis can be ignored. The results showed that the synthesis temperatures had a great influence on the photocatalytic performance of the

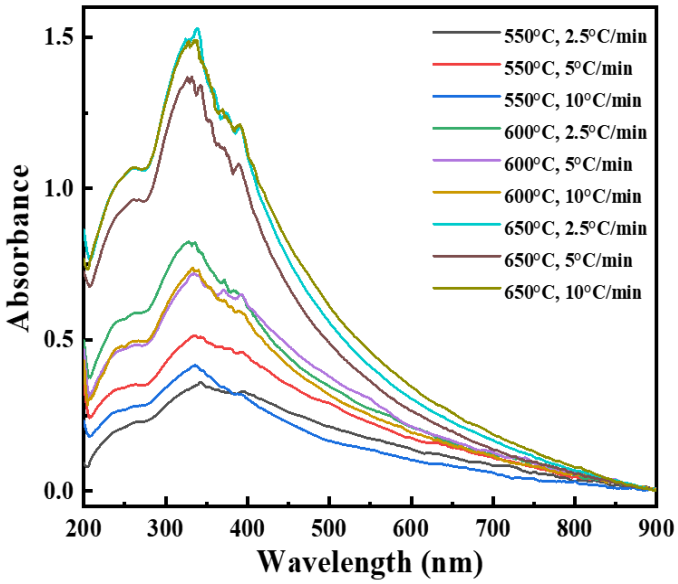

Fig. 6. UV-Vis–NIR absorption spectra of the synthesized g-C_3N_4 nanosheets as a function of pyrolysis temperature and heating rate

g-C_3N_4 nanosheets. The sample synthesized at 650°C exhibited the highest activity, 95.2% of MB was photodegraded in 120 min. For the samples prepared at 600°C and 550°C, only 83.7% and 74.6% MB were photodegraded in the same irradiation time, respectively. According to the UV-vis analysis, the increased photocatalytic activity can be attributed to the red shift of the absorption wavelength and the increased absorption intensity of visible light of the g-C_3N_4 synthesized at relatively high temperature through the change in the morphologies and crystal natures of the g-C_3N_4 nanosheets.

4. Conclusions

In this study, novel and versatile g-C_3N_4 nanosheets were synthesized by the simple thermal pyrolysis of urea at various pyrolysis temperatures and heating rates. The physicochemical and optical characteristics of the prepared g-C_3N_4 nanosheets were greatly influenced by the pyrolysis temperature rather than the

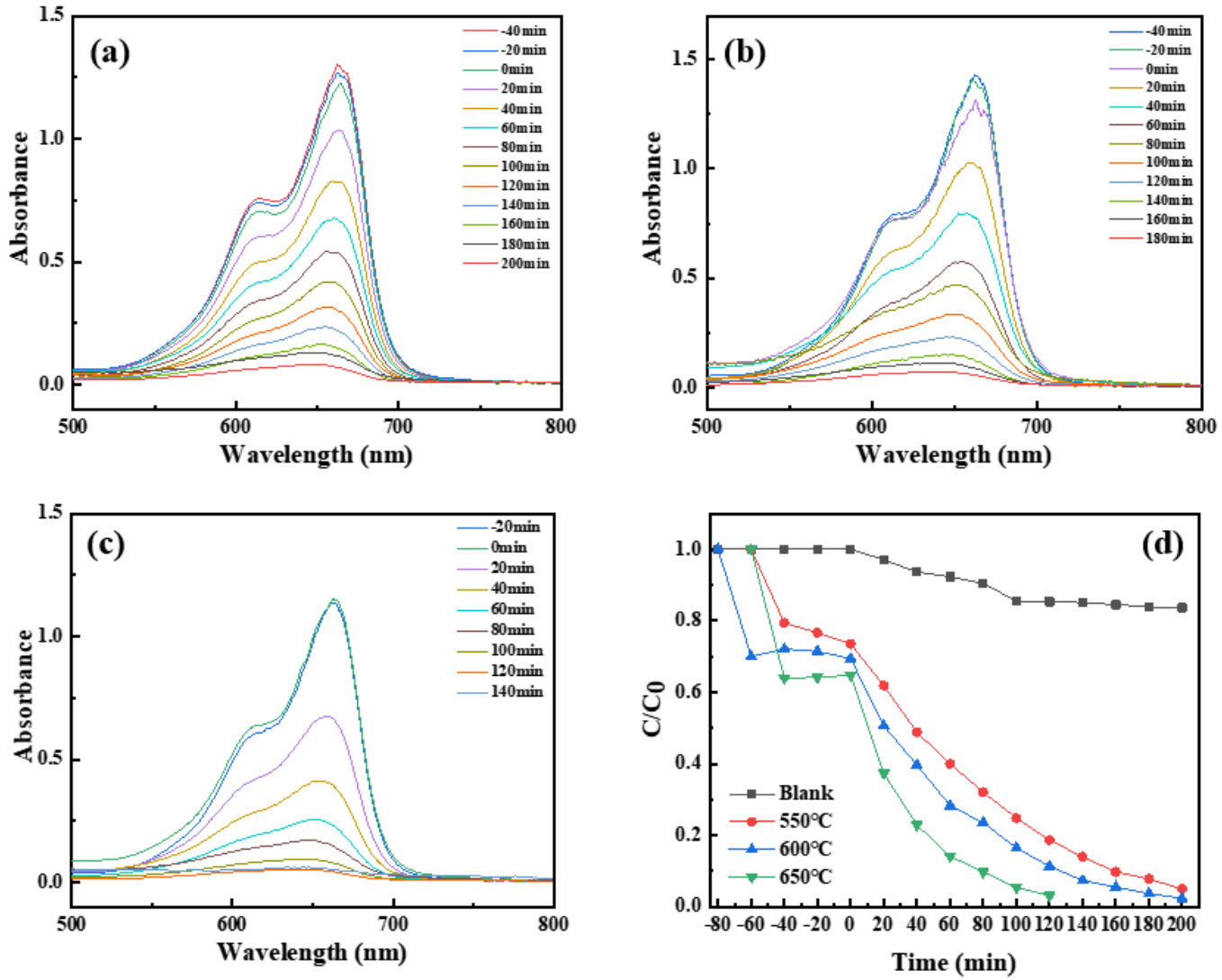

Fig. 7. UV-Vis spectral variation of MB solutions during photocatalytic degradation under visible light irradiation with the g-C_3N_4 nanosheets synthesized at different temperatures: (a) 550°C, (b) 600°C, (c) 650°C. (d) Relative concentration (C/C_0) of MB as a function of irradiation time in the presence of g-C_3N_4 nanosheets

heating rate. When synthesized at a relatively high temperature, the amount of material being synthesized is reduced, however it has been found to represent optical properties suitable for highly efficient photocatalyst by the increase in the thickness and defects formed in the g-C_3N_4 nanosheets. The photocatalytic degradation experiment of MB dyes indicated that the highest degradation of 95.2% after the reaction for 120 min was achieved on the g-C_3N_4 nanosheets synthesized at 650°C. This work may provide the suitable synthesis condition to develop novel and versatile g-C_3N_4 photocatalysts to treat industrial waste water containing organic pollutants.

Acknowledgments

This research was supported by Basic Science Research Program through the National Research Foundation (NRF) of Korea funded by the Ministry of Education (NRF-2018R1D1A1B07048149).

REFERENCES

[1] M.N. Chong, B. Jin, C.W.K. Chow, C. Saint, Water Res. **44**, 2997 (2010).
[2] I.K. Konstantinou, T.A. Albanis, Appl. Catal., B: Environ. **49**, 1 (2004).
[3] C. Chen, W. Ma, J. Zhao, Chem. Soc. Rev. **39**, 4206 (2010).
[4] M.A. Henderson, Surf. Sci. Rep. **66**, 185 (2011).
[5] M. Sachs, E. Pastor, A. Kafizas, J.R. Durrant, J. Phys. Chem. Lett. **7**, 3742 (2016).
[6] G. Fazio, L. Ferrighi, C.D. Valentin, Nano Energy **27**, 673 (2016).
[7] C. Chen, W. Ma, J. Zhao, Chem. Soc. Rev. **39**, 4206 (2010).
[8] G.-D. Lim, J.-H. Yoo, M. Ji, Y.-I. Lee, J. Alloys Compd. **806**, 1060 (2019).
[9] A. Malathi, J. Madhavan, M. Ashokkumar, P. Arunachalam, Appl. Catal., A: Gen. **555**, 47 (2018).
[10] Y. Lv, W. Yao, R. Zong, Y. Zhu, Sci. Rep. **6**, 19347 (2016).
[11] W. Xu, S. Zhu, Y. Liang, Z. Li, Z. Cui, X. Yang, A. Inoue, Sci. Rep. **5**, 18125 (2015).
[12] W.-J. Ong, L.-L. Tan, Y. H. Ng, S.-T. Yong, S.-P. Chai, Chem. Rev. **116**, 7159 (2016).
[13] J. Wen, J. Xie, X. Chen, X. Lia, Appl. Surf. Sci. **391**, 72 (2017).
[14] X.L. Wang, H.G. Yang, Appl. Catal., B: Environ. **205**, 624 (2004).
[15] H. Yoneyama, Y. Toyoguchi, H. Tamura, J. Phys. Chem. **76**, 3460 (1972).
[16] S.C. Yan, Z.S. Li, Z.G. Zou, Langmuir **25**, 10397 (2009).
[17] L. Ge, Mater. Lett. **65**, 2652 (2011).
[18] B.D. Cullity, Am. J. Phys. **25**, 394 (1957).